Nanocellulose-lysozyme colloidal gels via electrostatic complexation

Author(s):
Wu, Tingting; Kummer, Nico; De France, Kevin J.; Campioni, Silvia; Zeng, Zhihui; Siqueira, Gilberto; Dong, Jie

Publication date:
2021-01-01

Permanent link:
https://doi.org/10.3929/ethz-b-000441360

Originally published in:
Carbohydrate Polymers 251, https://doi.org/10.1016/j.carbpol.2020.117021

Carbohydrate Polymers 251 (2021) 117021

Contents lists available at ScienceDirect

Carbohydrate Polymers

journal homepage: www.elsevier.com/locate/carbpol

Nanocellulose-lysozyme colloidal gels via electrostatic complexation

Tingting Wu [a,b], Nico Kummer [a,c], Kevin J. De France [a], Silvia Campioni [a], Zhihui Zeng [a], Gilberto Siqueira [a], Jie Dong [b], Gustav Nyström [a,c,*]

[a] Laboratory for Cellulose & Wood Materials, Empa - Swiss Federal Laboratories for Materials Science and Technology, Überlandstrasse 129, 8600, Dübendorf, Switzerland

[b] State Key Laboratory for Modification of Chemical Fibers and Polymer Materials, College of Materials Science and Engineering, Donghua University, Shanghai, 201620, PR China

[c] Department of Health Science and Technology, ETH Zürich, Schmelzbergstrasse 9, CH-8092, Zürich, Switzerland

ARTICLE INFO

Keywords:
Cellulose nanofibrils
Lysozyme
Electrostatic complexation
Colloids
Rheology

ABSTRACT

Biohybrid colloids were fabricated based on electrostatic complexation between anionic TEMPO-oxidized cellulose nanofibrils (TO-CNF) and cationic hen egg white lysozyme (HEWL). By altering the loading of HEWL, physical colloidal complexes can be obtained at a relatively low concentration of TO-CNF (0.1 wt%). At neutral pH, increasing the HEWL loading induces an increase in charge screening, as probed by zeta-potential, resulting in enhanced TO-CNF aggregation and colloidal gel formation. Systematic rheological testing shows that mechanical reinforcement of the prepared biohybrid gels is easily achieved by increasing the loading of HEWL. However, due to the relatively weak nature of electrostatic complexation, the formed colloidal gels exhibit partial destruction when subjected to cyclic shear stresses. Still, they resist thermo-cycling up to 90 °C. Finally, the pH responsiveness of the colloidal complex gels was demonstrated by adjusting pH to above and below the isoelectric point of HEWL, representing a facile mechanism to tune the gelation of TO-CNF/HEWL complexes. This work highlights the potential of using electrostatic complexation between HEWL and TO-CNF to form hybrid colloids, and demonstrates the tunability of the colloidal morphology and rheology by adjusting the ratio between the two components and the pH.

1. Introduction

Proteins and polysaccharides are commonly used to construct biohybrid food-grade colloids because they are both naturally biocompatible and biodegradable (Huang et al., 2020; Pei, Li, McClements, & Li, 2019). Cellulose nanofibrils (CNF) are a class of abundant, sustainable, biocompatible and renewable biomass with a large range of remarkable properties, such as biodegradability, biocompatibility and renewability, as well as ease of functionalization (Arcari et al., 2019; De France, Hoare, & Cranston, 2017; De France, Zeng, Wu, & Nyström, 2020; Desmaisons, Boutonnet, Rueff, Dufresne, & Bras, 2017; Håkansson et al., 2014; Klemm et al., 2018). Among them, TEMPO-mediated oxidation of the hydroxyl groups on the surface of CNF is a widely reported method to introduce negatively charged carboxylate groups onto the CNF, here referred to as TO-CNF, resulting in new functionalities (Rol, Belgacem, Gandini, & Bras, 2019; Saito, Kimura, Nishiyama, & Isogai, 2007; Weishaupt et al., 2015). Several research efforts on TO-CNF have focused on its potential biomedical applications, such as drug delivery (Löbmann & Svagan, 2017) and wound healing (Xu et al., 2018), or as rheological modifier in inks for 3D printing (Shin et al., 2017).

Lysozyme is a natural antimicrobial enzyme widely found in eggs and animal secretions; specifically lysozyme from hen egg whites (HEWL) has attracted significant research attention due to its low cost and widespread availability (Eby, Schaeublin, Farrington, Hussain, & Johnson, 2009; Horn, Tracy, Easley, & Davis, 2012). Moreover, the isoelectric point of HEWL is 10.7, bearing a net positive charge over a broad pH range making it an ideal candidate to form colloidal complexes with negatively charged biomolecules (Syngai & Ahmed, 2019; Tiantian Wu et al., 2019). Furthermore, the intrinsic antimicrobial activity of lysozyme is often exploited in food packaging and wound healing applications, which demonstrates the multi-functionality of lysozyme (Barbiroli et al., 2012; Liu et al., 2019; Zhang, Zhou et al., 2015).

The combination of cellulose and HEWL has been previously investigated for medical and food science applications (Dekina, Romanovska, Ovsepyan, Tkach, & Muratov, 2016; Edwards, Prevost, Condon, & French, 2011). In particular, many researchers have investigated the

* Corresponding author.
E-mail address: gustav.nystroem@empa.ch (G. Nyström).

https://doi.org/10.1016/j.carbpol.2020.117021
Received 1 July 2020; Received in revised form 13 August 2020; Accepted 27 August 2020
Available online 1 September 2020

complexes and gels formed between sodium carboxymethyl cellulose (CMC) and HEWL based on electrostatic and hydrophobic interactions (Li et al., 2017; Li, Xu, Zhang, Chen, & Li, 2015; Pei et al., 2019; Zhu et al., 2013). Composite networks have been successfully formed through a variety of different complexation mechanisms, including covalent cross-linking (Tavakolian, Okshevsky, Van De Ven, & Tufenkji, 2018). For instance, positively charged lysozyme was incorporated into a paper matrix containing CMC via non-covalent binding for food packaging applications (Barbiroli et al., 2012). In another example, a Ca^{2+}-cross-linked TO-CNF hydrogel was investigated to act as a carrier for positively charged lysozyme for topical drug delivery applications, where the electrostatic interactions between lysozyme and the TO-CNF hydrogel structure played a key role for the efficient loading of the hydrogels (Basu, Strømme, & Ferraz, 2018). Moreover, lysozyme was immobilized to cellulose nanocrystals (CNC) by adsorption to carbodiimide-activated carboxylate groups in the surface of CNC, resulting in enhanced antibacterial activity (Abouhmad, Dishisha, Amin, & Hatti-Kaul, 2017). Finally, the combination of nanocellulose and lysozyme was evaluated in paper filters for advanced separation applications (Gustafsson, Manukyan, & Mihranyan, 2017). All these works have shown a great potential of exploiting the electrostatic interaction between anionic cellulose and cationic lysozyme for the formulation of novel bio-complexes.

The interaction of lysozyme with charged polymers is pH-dependent. For example, the changes in pH greatly influenced the formation of electrostatic complexes between lysozyme and low methoxyl pectin (Amara, Degraeve, Oulahal, & Gharsallaoui, 2017). Besides, the colloidal stability of pure TO-CNF gel networks is also controlled by pH (Alves et al., 2020; Fall, Lindström, Sundman, Ödberg, & Wågberg, 2011; Mendoza, Batchelor, Tabor, & Garnier, 2018), since under acidic conditions the carboxylic groups get protonated resulting in an aggregated CNF gel. The pH-responsiveness of TO-CNF hydrogels can be tuned by adjusting the negatively charged carboxyl density of the CNF during the TEMPO-mediated oxidation process (Masruchin, Park, & Causin, 2018) and is an attractive feature for the formulation of novel materials. Changes of pH can cause the dissociation or regeneration of hydrogel networks composed of phenylboronic acid-grafted alginate and PVA, due to the pH-responsiveness of phenylboronic acid-diol ester bonds, (Meng et al., 2014). Interestingly, pH-dependent dimerization of an engineered spidroin protein was exploited recently as a means to modulate the viscoelastic properties of protein-cellulose complexes (Voutilainen, Paananen, Lille, & Linder, 2019). Therefore, pH-responsiveness is a key point to investigate in the design of colloidal complexes between charged polymers.

To the best of our knowledge, there has been no report on the electrostatic complexation of TO-CNF and HEWL at low CNF concentrations (i.e. below the threshold to form a percolated gel network). Therefore, in this work a series of TO-CNF and HEWL complexes with different relative ratios were characterized. Effects of the loading of HEWL on the complexation process were evaluated in terms of zeta-potential, morphological and rheological properties. Moreover, the stability of the complexes was monitored under high shear stress, heating-cooling cycles, and changes in pH. Our results indicate that pH-dependent complexation of TO-CNF and HEWL can be used to formulate hybrid colloidal gels for possible applications in the food and medical industries, for instance as thickeners, stabilizers and gelling agents.

2. Experimental section

2.1. Materials

HEWL (hen egg white lysozyme, Mw =14.3 kDa), sodium hydroxide (NaOH), and (3-Aminopropyl) triethoxysilane (APTES) were purchased from Sigma-Aldrich. HEPES (4-(2-hydroxyethyl)-1-piperazineethanesulfonic acid), 2,2,6,6-Tetramethyl-1-piperidinyloxyl (TEMPO), and sodium hypochlorite (NaClO) solution (12–14 % chlorine) were obtained from VWR. Never-dried elemental chlorine free (ECF) cellulose fibers from bleached softwood pulp (Picea abies and Pinus app.) were obtained from Stendal GmbH (Berlin, Germany). Sodium bromide (NaBr $\geq$ 99 %) was supplied by Carl Roth GmbH & Co. All chemicals were used as received without any further purification.

2.2. Preparation of TEMPO-oxidized cellulose nanofibrils (TO-CNF)

TEMPO-mediated never dried cellulose fiber oxidation was performed following previously established protocols (Saito et al., 2007; Weishaupt et al., 2015) with slight modifications. Briefly, the never dried cellulose pulp (33.3 wt%), with a chemical composition of 81.3 % Cellulose, 12.6 % hemicellulose, 0% lignin and 0.3 % ash (Josset et al., 2014), was dispersed in distilled water to a final concentration of 2 wt%. TEMPO and NaBr were dissolved in water at ratios of 0.1 and 1.0 mmol/g of cellulose pulp respectively, and were then mixed with the cellulose pulp dispersion. The pH of the suspension was then adjusted to 10–10.5 using 2 wt% NaOH. 10 mmol NaClO was then added per gram of cellulose. The reaction was allowed to proceed at room temperature for 4−5 h, after which the TEMPO-oxidized cellulose fibers were washed several times with distilled water until the conductivity was close to that of distilled water, and subsequently ground using a Supermass Colloider (MKZA10-20 J CE Masuko Sangyo, Japan) at an applied energy of 9 kW h/kg. The ground CNF was further fibrillated using a high shear homogenizer (M-110EF, Microfluidics Ind., Newton, MA-USA) for a total of 10 passes at a pressure of 8 bar. After homogenization, a uniform and transparent TO-CNF dispersion (Fig. S1) with a concentration of 0.5 $\pm$ 0.1 wt% was obtained.

2.3. Preparation of TO-CNF and HEWL complexes

A stock solution of HEWL was dissolved in 10 mM HEPES buffer (final concentration $\sim$ 2.2 mg/mL) and the pH was adjusted to 7.4–7.5 using 1 M NaOH. The HEWL solution in HEPES buffer was then passed through a 0.2 μm cellulose acetate syringe filter to remove any aggregates. Subsequently, 0.5 wt% TO-CNF in water was mixed with a specified amount of HEWL, yielding a final concentration of TO-CNF of 0.1 wt% (1 mg/mL) and a final concentration of HEWL between 0 and 0.1 wt % (10:1 – 10:10 wt ratio of TO-CNF:HEWL). 0.1 wt% TO-CNF only (denoted 10:0) and 0.1 wt% HEWL only (denoted 0:10) samples were also prepared as controls. Specifically, a volume of 30 mL of TO-CNF and HEWL was obtained by mixing 6 mL of 0.5 wt% TO-CNF in MilliQ, 9 mL of MilliQ, and the required amount of HEWL stock solution in 15 mL of HEPES buffer, ensuring the same ionic strength in each biohybrid mixture. Similarly, for pure HEWL suspensions, 6 mL 0.5 wt% TO-CNF was replaced by 6 mL of MilliQ, such that the final concentration of HEWL was kept at 1 mg/mL. For pure TO-CNF suspensions, 15 mL HEPES buffer was added without any HEWL. Samples were allowed to equilibrate for 1 week under ambient conditions before further characterization.

2.4. Characterization

Attenuated Total Reflection-Fourier Transform Infra-Red (ATR-FTIR) measurements were performed on a Tensor 27 spectrometer (Bruker Switzerland AG) over the wavenumber range from 500 to 4000 cm^{-1}. Circular Dichroism (CD) testing was performed on a JASCO J-815 CD spectrometer, using a 1 mm cuvette. Here, the selected mixtures were diluted by a factor of 3 prior to CD measurements. Morphology of TO-CNF and HEWL biohybrid complexes were characterized by high-resolution transmission electron microscopy (HRTEM, JEOL, JEM 2200fS), atomic force microscopy (AFM, Bruker ICON3) and field-emission scanning electron microscopy (FESEM, Fei Nova Nanosem 230). For AFM measured in tapping mode, note that all samples contain the same concentration of TO-CNF and were deposited onto a freshly

cleaved mica substrate, modified with 0.05 % APTES prior to imaging (note that due to their positive charge, pure HEWL samples were deposited onto an unmodified substrate). TEM images were obtained after the complexes (0.001 wt%) were deposited, stained by 1 wt% uranyl acetate and dried on copper grids coated with carbon. Zeta-potential measurements were performed at 25 °C using a suspension concentration of 0.005 wt% (Malvern, zetasizer nano series). pH values were measured at room temperature (METTLER TOLEDO, SevenEasy). Rheological testing was performed with an Anton Paar MCR302 rheometer using a double gap cylinder geometry (STANDARD MEASURING SYSTEM DG26.7/T200/SS) at 25 °C for both oscillatory and rotational measurements. For the double gap cylinder, the internal and external diameter are 23.830 mm and 27.593 mm, respectively. Turbidity measurements were acquired from the Transmittance at 600 nm by using a Cary UV–vis spectrophotometer. Optical microscopy images were obtained from a Leica DFC420 Microscope.

3. Results and discussion

TO-CNF and HEWL biohybrid colloids were formed on the basis of electrostatic complexation between negatively charged TO-CNF and positively charged HEWL. This is analogous to previous studies where negatively charged nanocellulose-based matrices have been shown to act as an efficient adsorbent for positively charged proteins such as lysozyme (Anirudhan & Rejeena, 2012; Dutta, Samanta, & Dhara, 2016). In Fig. 1**(a)**, the electrostatic interaction process is illustrated for increasing concentrations of HEWL. With no added HEWL, a stable and homogenous TO-CNF suspension is formed, due to the existence of repulsive forces between the negatively charged carboxylate groups arising from the TEMPO-mediated oxidation. The addition of positively charged HEWL leads to adsorption directly to the negatively charged TO-CNF surfaces via electrostatic complexation, thus reducing the CNF colloidal stability via charge screening. However, at relatively low HEWL concentrations (up to ca. 10:4 of CNF to HEWL mass ratio) the degree of complexation is not yet sufficient to form a stable gel-like network. After the addition of a sufficiently high concentration of HEWL (above ca. 10:5 mass ratio), enhanced charge screening leads to the aggregation of TO-CNF into clusters in the size range of a few hundreds of microns (Fig. 1(d)). Herein, we focus on understanding the fundamentals of the interactions between TO-CNF and HEWL, while simultaneously investigating the effects of the ratio between positively charged HEWL and negatively charged TO-CNF on the characteristics of the resulting biohybrid colloids.

Scanning electron microscopy (SEM) (Fig. 1(b and c)) and optical microscopy (Fig. 1(d)) were used to visualize the association between TO-CNF and HEWL. Note that in the case of pure TO-CNF suspensions, a relatively uniform fibrillar network is apparent, whereby upon the addition of HEWL, this network largely collapses. However, due to the relatively small hydrodynamic radius of HEWL (ca. 2.0 nm) (Gull, Ishtikhar, Alam, Sabah Andrabi, & Khan, 2017), it is challenging to visualize its distribution within the final complexes via SEM. The complexes obtained at mass ratio values higher than 10:5 are on the order of hundreds of micrometers, and relatively irregular in shape.

As surface charge chemistry and density are largely responsible for the formation of stable colloidal systems (Zhu et al., 2020), the zeta potential of the TO-CNF/HEWL complexes was measured (Fig. 2). HEWL, with an isoelectric point of 10.7, is positively charged under physiological pH (zeta potential of +13.9 mV), while TO-CNF is negatively charged (zeta potential of -57.0 mV), demonstrating a strong potential for electrostatic complexation. At lower concentrations of HEWL (10:0 to 10:3), there is little change in the overall zeta potential due to the strongly negative nature of TO-CNF and limited charge screening (Fig. 2). As the concentration of HEWL is further increased (from 10:3 to 10:10), the zeta potential begins to increase accordingly, indicative of increased charge screening. Correspondingly, an increase in suspension turbidity and aggregation becomes apparent from a TO-CNF:HEWL ratio of 10:4, whereby with further increasing HEWL concentration, the aggregation becomes more pronounced. By comparison, pure TO-CNF and HEWL suspensions with the same concentration (1 mg/mL) are transparent (Fig. S1), implying that any observed turbidity/aggregation arises solely due to electrostatic complexation between the two oppositely charged biomolecules. Notably, the interaction between various positively charged biomolecules and negatively charged TO-CNF has shown a strong dependency on the ionic strength and pH value of the suspension mixture (Anirudhan & Rejeena, 2012; Pei et al., 2019; Weishaupt et al., 2015; Wu, Zeng, Siqueira, & De France, 2020). Since the pH of the solution remained relatively constant across all ratios of TO-CNF:HEWL (Fig. 2b), we can conclude that the electrostatic interactions between TO-CNF and HEWL are the cause of the appearance of these aggregates/flocs, without the requirement of

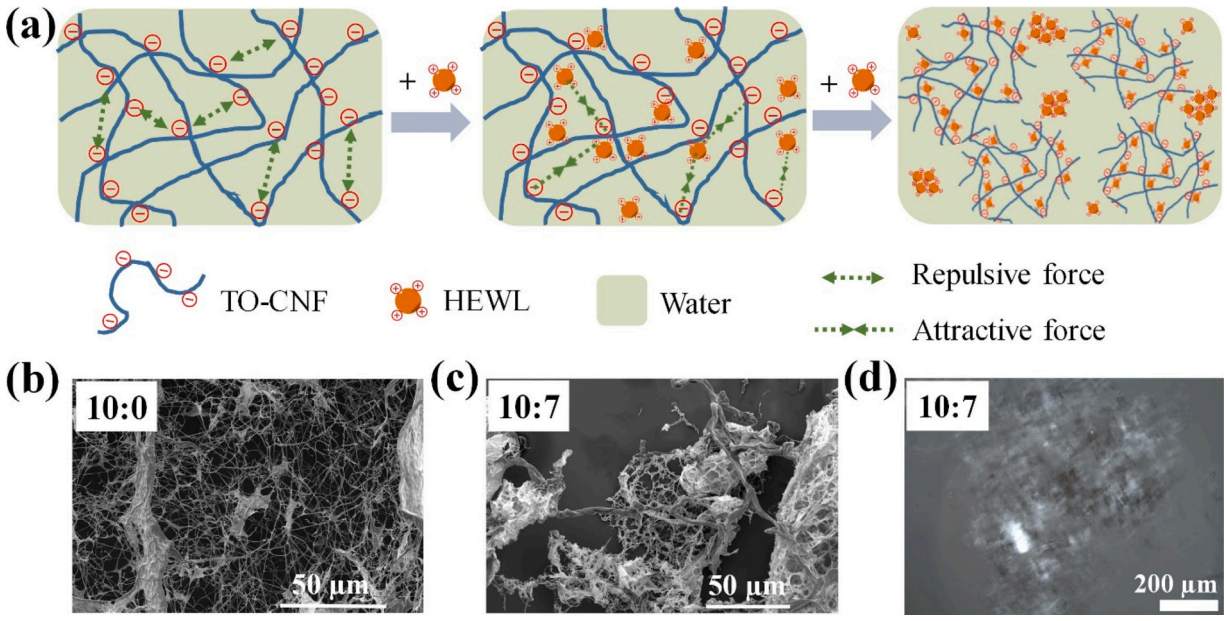

Fig. 1. (a) Schematic illustration of the interaction mechanism between TO-CNF and HEWL upon increasing the HEWL loading; (b and c) SEM images of pure TO-CNF and TO-CNF and HEWL colloidal complexes (10:7 relative mass ratio); (d) Optical microscope image of TO-CNF and HEWL colloids (10:7 relative mass ratio).

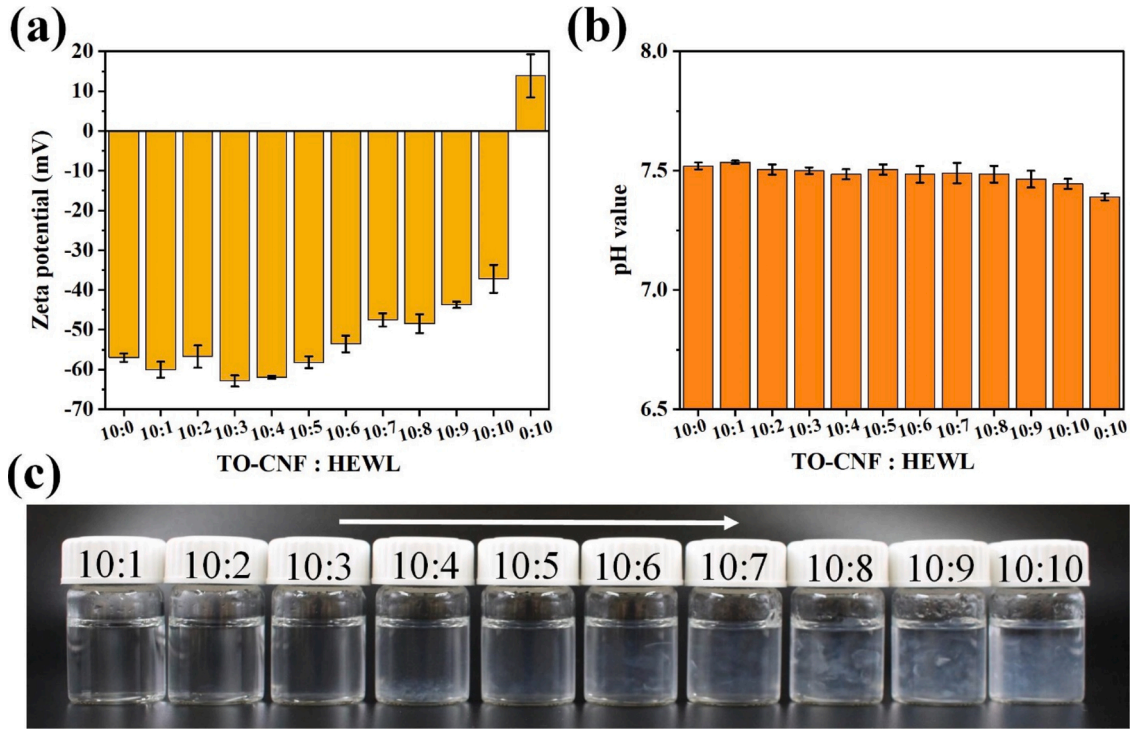

Fig. 2. (a) Zeta-potential, (b) pH value and (c) photographs of TO-CNF and HEWL colloidal complexes with different ratios between TO-CNF and HEWL (10:0 to 0:10).

any chemical or heat treatments. Further turbidity analysis is shown in Fig. S2, demonstrating that turbidity increases as HEWL loading is also increased (the same trend seen in the photographs).

FTIR spectroscopy is a conventional method to investigate the conformational changes in secondary structure of proteins (Mallamace, Fazio, Mallamace, & Corsaro, 2018; Sudhakar, Santhosh, & Mani, 2017). The binding of HEWL to negatively charged lipid vesicles leads to conformational changes and subsequent aggregation of the protein (Al Kayal et al., 2012). Herein, the effect of TO-CNF on the secondary structure of HEWL was investigated by means of ATR-FTIR. Pure HEWL shows two strong peaks, one at 1650 cm^{-1}, attributed to α-helices, and one at 1534 cm^{-1}, due to NH— bending of the peptide chains (Fig. 3). In pure TO-CNF, the peak at 1600 cm^{-1} is attributed to the COONa group on the TO-CNF surface after TEMPO oxidization. For 10:5 and 10:10 formulations, the two peaks at ~ 1650 and 1534 cm^{-1} are still apparent,

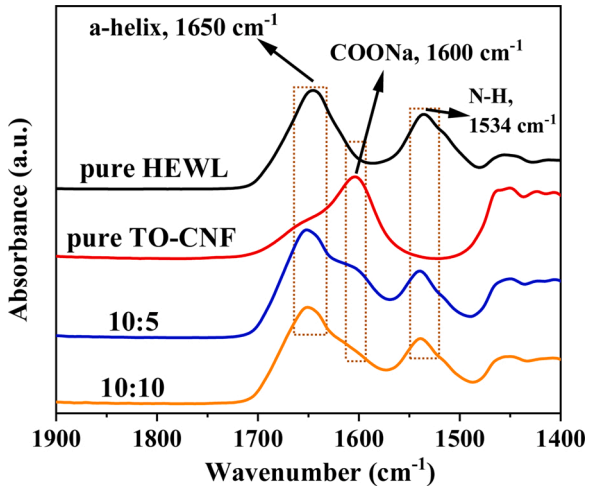

Fig. 3. ATR-FTIR spectra of TO-CNF and HEWL casted films with different ratios.

and with a little shift, indicating the successful incorporation of HEWL into TO-CNF and that the secondary structure of HEWL is stable and not significantly affected by the interaction with TO-CNF. In addition, CD measurements (Fig. S3) supported the presence of α-helices in the TO-CNF and HEWL colloidal systems. Of note, the signal of α-helices from HEWL in the colloidal systems is significantly decreased upon gel formation, indicating the presence of less 'free' HEWL in the suspensions, especially for 10:7 and 10:10 ratios.

TEM was performed to confirm the microstructure of the TO-CNF/HEWL colloids at various HEWL loadings (Figs. 4 and S4). Generally, the TEM images are in good agreement with the results seen via AFM. For pure TO-CNF suspensions, the individual cellulose nanofibers show uniform diameters of 3–4 nm with a length on the order of hundreds of nm. Upon the addition of HEWL (starting from a ratio of 10:3), no obvious differences between pure TO-CNF (10:0) are noticed. Increasing the HEWL concentration further, starting from 10:5, the TO-CNF tends to aggregate into nanofiber clusters, with similar structures also observed at 10:7.

AFM images were acquired at selected TO-CNF:HEWL ratios (10:0, 10:3, 10:5, 10:7 and 10:10), in order to gain an understanding of the evolution of the microstructure within these biohybrid colloids with increasing HEWL concentration (Figs. 5, S5 and S6). Individual nanofibers are readily observed in the pure TO-CNF (10:0) sample, as expected (Fig. S5). Individual filaments are also evident at low HEWL concentrations (10:3), again suggesting that the extent of charge screening caused by TO-CNF/HEWL electrostatic interaction is not enough to form colloids below a certain threshold concentration (Fig. 5). However, as the HEWL concentration is further increased, starting from 10:5, the TO-CNF start to entangle and aggregate together, indicative of significant charge screening (link to figure). At even higher HEWL loadings (10:7), the size of TO-CNF clusters begins to increase drastically (link). We hypothesize that at these high loadings, the biohybrid colloidal complexes become so big that most of the material precipitates out of suspension (Fig. 2(c)), and is thus not observable via AFM.

It is well known that the morphological properties of CNF suspensions affect their rheological behavior (Albornoz-Palma, Betancourt,

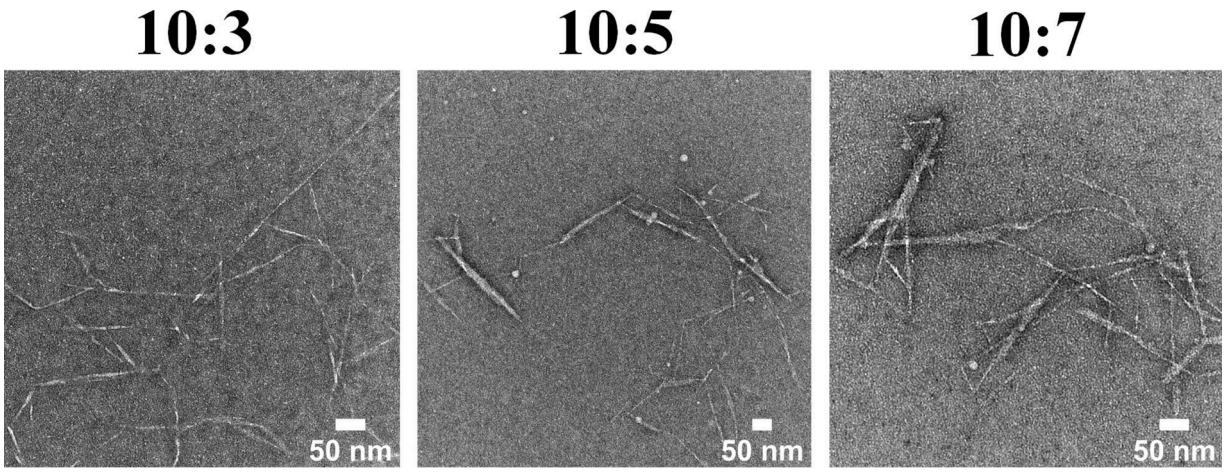

Fig. 4. TEM images of TO-CNF and HEWL colloidal complexes with different relative mass ratios (10:3, 10:5 and 10:7).

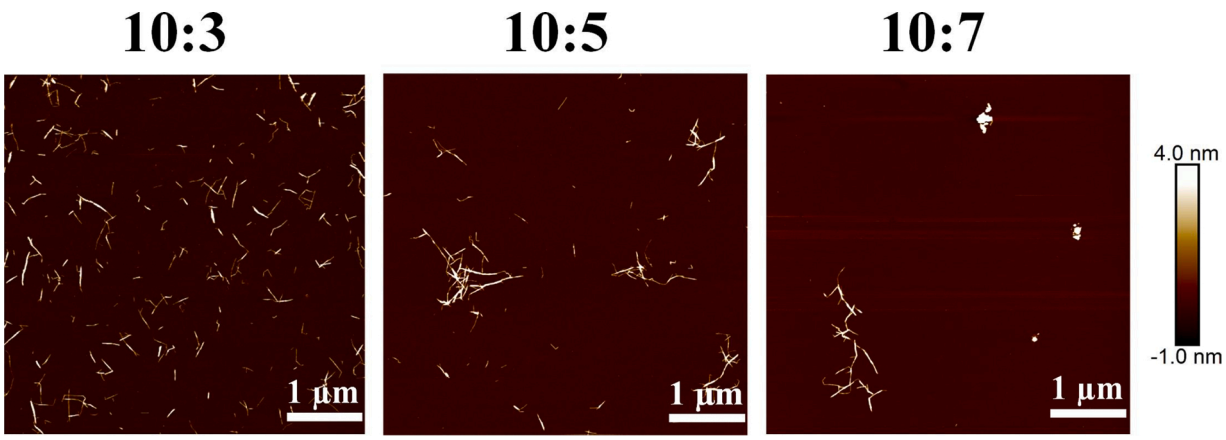

Fig. 5. AFM images of TO-CNF and HEWL colloidal complexes with different relative mass ratios (10:3, 10:5 and 10:7).

Mendonça, Chinga-Carrasco, & Pereira, 2020). Therefore, the rheological properties of the prepared biohybrid colloidal dispersions were studied in detail to gain an understanding of the stability of these colloids as well as their possibility to undergo a sol-gel transition. As with previous experiments, here we focus on the effects of HEWL loading on the rheological properties of the formed complexes at a fixed concentration of TO-CNF (0.1 wt%). Generally, during strain sweep measurements the crossover point of G' and G" can be defined as the apparent yield point, where G' represents the storage modulus and G" represents the loss modulus, which give a measure of the elasticity and viscosity of a material, respectively (Alves et al., 2020; Mendoza et al., 2018). All strain sweep measurements were performed from a strain of 0.01%–100 % at a constant angular frequency of 10 rad/s (Fig. 6**(a)**). For biohybrid colloidal dispersions with high HEWL loadings (starting from 10:5), there is a crossover of the G' and G" curves, indicating that with increasing the concentration of positively charged HEWL, the electrostatic interactions are enhanced, promoting the formation of a gelled network. Further increasing the HEWL concentration results in an increase in G' and in complex viscosity (Fig. 6(b)), suggesting the formation of a stronger viscoelastic network and gel-like structure due to enhanced electrostatic interaction throughout the system. Note that for all formulations, a linear viscoelastic region exists up to ~ 10 % strain, after which further increasing the strain results in a significant decrease of both G' and G", until an eventual crossover point is reached, indicating the destruction/yield of the gel networks and a gel-sol transition. Note that for complexes from 10:1 to 10:4, pure TO-CNF and HEWL, no gelation point is observed via rheology (Supporting Information, Figs. S7 and S8).

Frequency sweep tests are widely used to obtain information about the stability of 3D entangled networks in gel and colloidal systems (Zhang, Sun et al., 2015). Herein, frequency sweeps were performed from 0.01–100 rad/s under a constant strain of 1 % (within the linear viscoelastic region identified via strain sweep, Fig. 6(c)). Above TO-CNF: HEWL ratios of 10:5, all formulations show a single plateau region in the dynamic modulus (G' and G"), with G' dominating over G", indicative of a gelled/solid-like behavior. For the 10:5 complex, in the low frequency range the rheological behavior is similar to that of the other formulations, however at increased frequencies G' suddenly drops dramatically, representing liquid-like behavior and partial destruction of the entangled networks.

Additionally, cyclic rotation tests were performed to investigate the stability of these colloidal gels under cyclic shear force (Fig. 6(d)). Notably, the apparent viscosity decreases with increasing shear rate, depicting shear-thinning behavior, which is typical for CNF systems (Alves et al., 2020). Within the first cycle, there is already a large decrease in apparent viscosity, indicating partial destruction of the TO-CNF/HEWL gel networks (data shown for 10:7). The apparent viscosity appears to be relatively stable for up to 3 cycles however. Similar trends were observed for 10:10 (Fig. S9). Notably, for pure TO-CNF suspensions, this significant decrease in viscosity is not evident (Fig. S10), which is expected due to the lack of any gelled colloidal network. Importantly, the apparent viscosity for both 10:7 and 10:10 is still far higher than the apparent viscosity of pure TO-CNF after cyclic shearing, indicating only a partial (and not full) destruction of the gelled networks. Shear viscosity prior to cyclic testing for 10:10, 10:7, and 10:0 can be seen in Fig. 6(f).

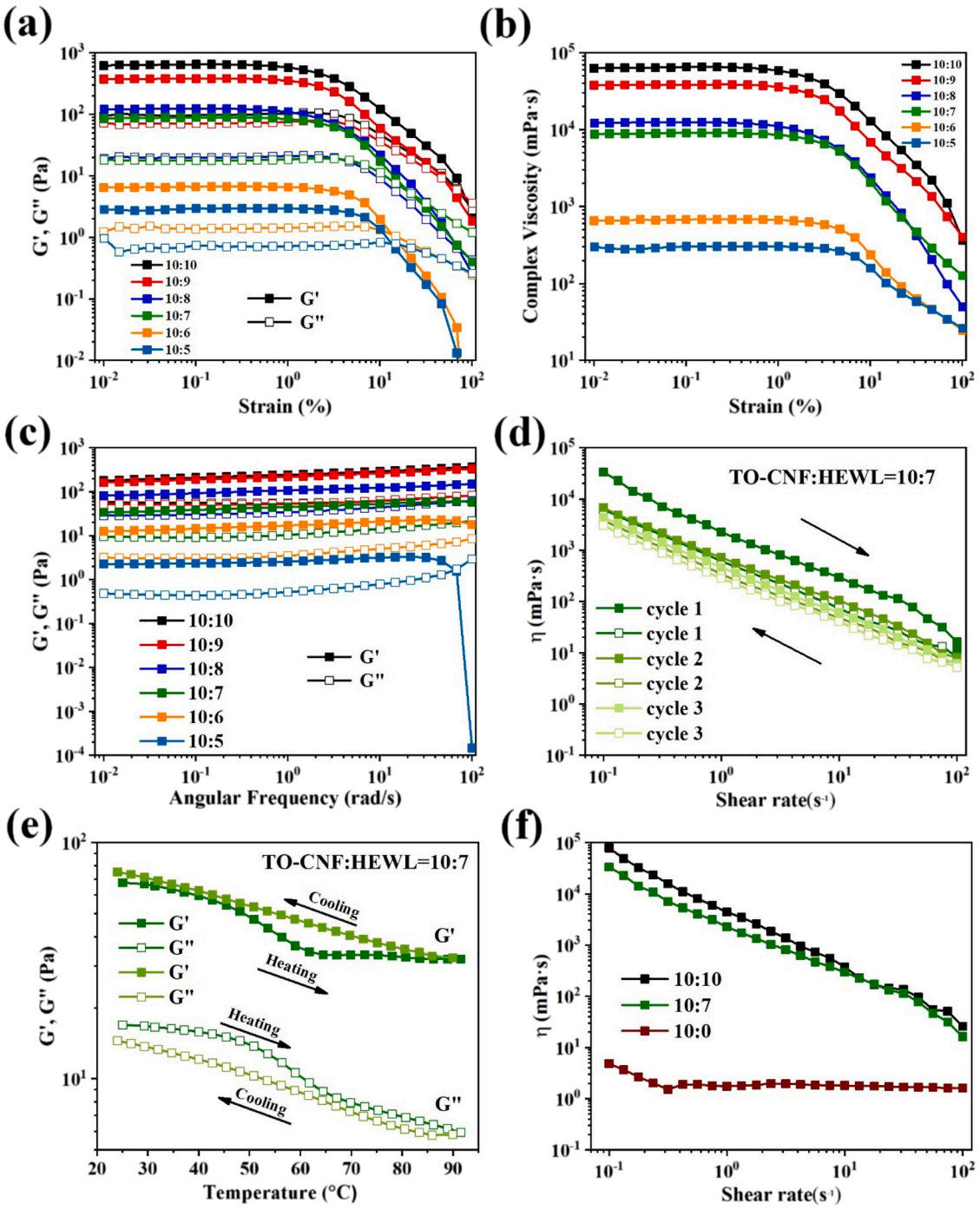

Fig. 6. Rheological properties of TO-CNF and HEWL colloidal systems at 25 ℃ with different ratios from 10:5 to 10:10, (a) storage modulus G' (solid) and loss modulus G" (open) on strain sweep at 10 rad/s, (b) complex viscosity at 10 rad/s, (c) dynamic frequency sweep (γ = 1%). (d) Shear viscosity loop of TO-CNF and HEWL colloids (TO-CNF:HEWL = 10:7), the increase and decrease of the shear rate (s^{-1}) is indicated by the arrows. (e) The values of both modulus of TO-CNF and HEWL complex (TO-CNF:HEWL = 10:7) during heating (dark green) and cooling (light green) cycles are displayed, storage modulus G' (solid) and loss modulus G" (open). (f) Shear viscosity of TO-CNF and HEWL colloids with different ratios (10:0, 10:7 and 10:10) (For interpretation of the references to colour in this figure legend, the reader is referred to the web version of this article).

Previous work has shown that proteins like HEWL are sensitive to heat treatments and generally show a heat-induced gelation behavior (Li et al., 2018). Therefore, the thermo-stability of the colloids was inspected by cyclic heating and cooling from 25 to 90 °C at a heating rate of 3 °C/min (Fig. 6(e)), where the G' and G" were recorded under fixed frequency (10 rad/s) and strain (1 %). Notably, upon increasing the temperature to 90 °C, both G' and G" decrease dramatically; conversely upon decreasing the temperature from 90 to 25 °C, both G' and G" increase dramatically. However, during the whole cycle, the G' values are always higher than the G" values, implying that the networks still exist in a gel-like state during the imposed heat treatment. The thermal-stability of pure HEWL was also characterized (Fig. S11) and the measured G' was always lower than G", suggesting a more liquid-like behavior. Furthermore, only a minor change in both G' and G" is observed as a result of thermal cycling, which is different from the change occurring in the complex systems, likely indicating that the

changes observed within the TO-CNF/HEWL complexes are primarily due to varied electrostatic interactions attributed to the increased mobility of TO-CNF and HEWL with increased temperature and not due to protein denaturation.

Moreover, the time-dependency of gel complexation was investigated visually and by rheological characterization for 10:7 (Fig. S12). Immediately after mixing, the gel complexes appear more homogeneous, and then after 1 week bigger flocs are readily observed, indicating increased aggregation/charge screening. In this state, the colloidal gels are then relatively stable, after which no significant visual changes are observed. In addition, although 10:7 demonstrates a gel-like behavior (with G' > G") both instantaneously and after 1 week in suspension, the modulus does increase over time, supporting the formation of a stronger/more prominent gel network with increased aggregation.

Previous studies have demonstrated that the electrostatic complexation between charged colloids depends on the pH of the solution (Alves et al., 2020; Kim, Late, Banga, Ludovice, & Prausnitz, 2008; Mendoza et al., 2018). Therefore, we analyzed the effects of changing the pH of the TO-CNF:HEWL mixtures at a fixed mass ratio of 10:7. The strain sweep curves measured at pH 12 (above the isoelectric point of HEWL) indicate that the complex shows a predominantly liquid-like behavior, due lack of binding between negatively charged HEWL and equally charged TO-CNF (Fig. 7**(a)**). Lowering the pH to 7.5 results in a significant increase in G', attributed to renewed complexation between oppositely charged TO-CNF and HEWL. Further lowering the pH to 3 results in an even higher increase in G', due to higher density of positive charges on HEWL, and increased TO-CNF aggregation due to protonation of carboxylic groups; similar observations have been seen in other systems with TO-CNF and polyacrylic acid derivatives (Alves et al., 2020, 2015).

The photographs in Fig. 7(b) demonstrate that as the pH is decreased from 12 to 3, the turbidity of the TO-CNF and HEWL complexes increases, indicative of increased aggregation. Moreover, this phenomenon is completely reversible, as demonstrated in Fig. 7(c), whereby turbidity is decreased upon sequential increase in pH to 12. We envision that these pH-switchable complexes could be useful for several potential applications, such as in cosmetic gels, and rheological modifiers for the food industry, where the colloidal properties can be easily controlled by adjusting the overall pH of the system. In particular, the ability to readily control suspension aggregation and rheological properties gives a level of flexibility which would be beneficial for matching targeted material properties.

4. Conclusion

In conclusion, a series of TO-CNF and HEWL colloids with different ratios were fabricated via simple electrostatic complexation between positively charged HEWL and negatively charged TO-CNF. Increasing the overall HEWL concentration within the colloidal complexes resulted in an increase in zeta potential (absolute value closer to 0) due to enhanced charge screening. Above HEWL concentrations of 10:5, TO-CNF and HEWL were prone to aggregation, attributed to the electrostatic attraction between opposite charges, evidenced via AFM and TEM. This aggregation resulted in noticeable differences in rheological properties, whereby complexes above HEWL loadings of 10:5 demonstrated gel-like properties, with G' values greater than G" values. The obtained colloids show a shear-thinning behavior and are relatively stable upon heating up to 90 °C. Importantly, this electrostatic complexation between HEWL and TO-CNF is pH-dependent; at a pH above the isoelectric

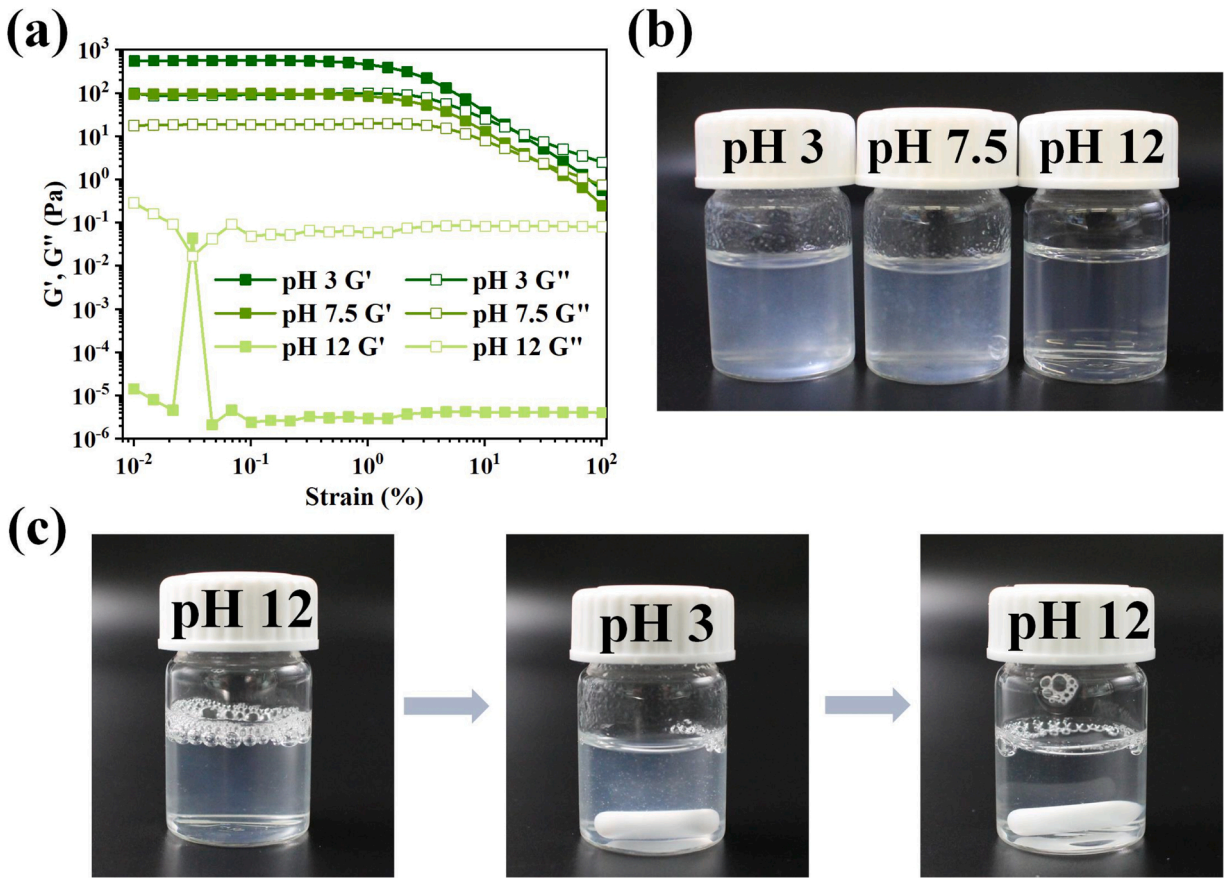

Fig. 7. Rheological properties of TO-CNF and HEWL colloids (TO-CNF:HEWL = 10:7) at 25 ℃ with different pH 3, 7.5 and 12 (a) storage modulus G' (solid) and loss modulus G" (open) on strain sweep at 10 rad/s; (b) photographs of the colloidal systems at different pH; (c) the colloidal complexes with changed pH, first from 12 to 3, then from 3 back to 12.

point of HEWL whereby HEWL is not positively charged, there is no interaction and therefore no colloidal formation. Decreasing the pH to below the isoelectric point of HEWL triggers complexation between the positively charged HEWL and negatively charged TO-CNF, resulting in flocculation and gelation. Importantly, the pH of the solution can be used to drive reversible formation and the dissolution of the colloids as in stimulus responsive gel systems. Overall, this work provides insights for understanding and utilizing the charge interactions between TO-CNF and HEWL and their responsiveness to changes in environmental conditions such as pH for a variety of potential applications ranging from drug delivery, 3D printing, packaging films to wound dressing.

CRediT authorship contribution statement

Tingting Wu: Conceptualization, Methodology, Investigation, Formal analysis, Writing - original draft. **Nico Kummer:** Investigation, Formal analysis, Writing - review & editing. **Kevin J. De France:** Conceptualization, Methodology, Writing - review & editing. **Silvia Campioni:** Conceptualization, Methodology, Writing - review & editing. **Zhihui Zeng:** Validation, Writing - review & editing. **Gilberto Siqueira:** Validation, Writing - review & editing. **Jie Dong:** Writing - review & editing, Supervision. **Gustav Nyström:** Conceptualization, Writing - review & editing, Supervision.

Declaration of Competing Interest

There are no conflicts to declare.

Acknowledgements

T.W. is supported by the China Scholarship Council (CSC) Fellowship. K.D. acknowledges funding from the Natural Sciences and Engineering Research Council of Canada (NSERC) Postdoctoral Fellowship program. We thank Anja Huch for help with TEM and SEM imaging. We thank Tutu Sebastian and Frank Clemens for help with rheological testing.

Appendix A. Supplementary data

Supplementary material related to this article can be found, in the online version, at doi:https://doi.org/10.1016/j.carbpol.2020.117021.

References

Abouhmad, A., Dishisha, T., Amin, M. A., & Hatti-Kaul, R. (2017). Immobilization to positively charged cellulose nanocrystals enhances the antibacterial activity and stability of Hen Egg White and T4 lysozyme. *Biomacromolecules, 18*(5), 1600–1608. https://doi.org/10.1021/acs.biomac.7b00219.

Al Kayal, T., Nappini, S., Russo, E., Berti, D., Bucciantini, M., Stefani, M., … Baglioni, P. (2012). Lysozyme interaction with negatively charged lipid bilayers: Protein aggregation and membrane fusion. *Soft Matter, 8*(16), 4524–4534. https://doi.org/10.1039/c2sm06906g.

Albornoz-Palma, G., Betancourt, F., Mendonça, R. T., Chinga-Carrasco, G., & Pereira, M. (2020). Relationship between rheological and morphological characteristics of cellulose nanofibrils in dilute dispersions. *Carbohydrate Polymers, 230*(November 2019), Article 115588. https://doi.org/10.1016/j.carbpol.2019.115588.

Alves, L., Ferraz, E., Lourenço, A. F., Ferreira, P. J., Rasteiro, M. G., & Gamelas, J. A. F. (2020). Tuning rheology and aggregation behaviour of TEMPO-oxidised cellulose nanofibrils aqueous suspensions by addition of different acids. *Carbohydrate Polymers, 237*(February), Article 116109. https://doi.org/10.1016/j.carbpol.2020.116109.

Alves, Luís, Lindman, B., Klotz, B., Böttcher, A., Haake, H. M., & Antunes, F. E. (2015). Rheology of polyacrylate systems depends strongly on architecture. *Colloid and Polymer Science, 293*(11), 3285–3293. https://doi.org/10.1007/s00396-015-3715-4.

Amara, C. B., Degraeve, P., Oulahal, N., & Gharsallaoui, A. (2017). pH-dependent complexation of lysozyme with low methoxyl (LM) pectin. *Food Chemistry, 236*, 127–133. https://doi.org/10.1016/j.foodchem.2017.03.124.

Anirudhan, T. S., & Rejeena, S. R. (2012). Poly(acrylic acid)-modified poly (glycidylmethacrylate)-grafted nanocellulose as matrices for the adsorption of lysozyme from aqueous solutions. *Chemical Engineering Journal, 187*, 150–159. https://doi.org/10.1016/j.cej.2012.01.113.

Arcari, M., Zuccarella, E., Axelrod, R., Adamcik, J., Sánchez-Ferrer, A., Mezzenga, R., … Nyström, G. (2019). Nanostructural properties and twist periodicity of cellulose nanofibrils with variable charge density. *Biomacromolecules, 20*(3), 1288–1296. https://doi.org/10.1021/acs.biomac.8b01706.

Barbiroli, A., Bonomi, F., Capretti, G., Iametti, S., Manzoni, M., Piergiovanni, L., … Rollini, M. (2012). Antimicrobial activity of lysozyme and lactoferrin incorporated in cellulose-based food packaging. *Food Control, 26*(2), 387–392. https://doi.org/10.1016/j.foodcont.2012.01.046.

Basu, A., Strømme, M., & Ferraz, N. (2018). Towards tunable protein-carrier wound dressings based on nanocellulose hydrogels crosslinked with calcium ions. *Nanomaterials, 8*(7). https://doi.org/10.3390/nano8070550.

De France, K. J., Hoare, T., & Cranston, E. D. (2017). Review of hydrogels and aerogels containing nanocellulose. *Chemistry of Materials, 29*(11), 4609–4631. https://doi.org/10.1021/acs.chemmater.7b00531.

De France, K., Zeng, Z., Wu, T., & Nyström, G. (2020). Functional materials from Nanocellulose: Utilizing structure–Property relationships in bottom-up fabrication. *Advanced Materials*. , Article 2000657. https://doi.org/10.1002/adma.202000657.

Dekina, S., Romanovska, I., Ovsepyan, A., Tkach, V., & Muratov, E. (2016). Gelatin/carboxymethyl cellulose mucoadhesive films with lysozyme: Development and characterization. *Carbohydrate Polymers, 147*, 208–215. https://doi.org/10.1016/j.carbpol.2016.04.006.

Desmaisons, J., Boutonnet, E., Rueff, M., Dufresne, A., & Bras, J. (2017). A new quality index for benchmarking of different cellulose nanofibrils. *Carbohydrate Polymers, 174*, 318–329. https://doi.org/10.1016/j.carbpol.2017.06.032.

Dutta, S., Samanta, P., & Dhara, D. (2016). Temperature, pH and redox responsive cellulose based hydrogels for protein delivery. *International Journal of Biological Macromolecules, 87*, 92–100. https://doi.org/10.1016/j.ijbiomac.2016.02.042.

Eby, D. M., Schaeublin, N. M., Farrington, K. E., Hussain, S. M., & Johnson, G. R. (2009). Lysozyme catalyzes the formation of antimicrobial silver nanoparticles. *ACS Nano, 3*(4), 984–994. https://doi.org/10.1021/nn900079e.

Edwards, J. V., Prevost, N. T., Condon, B., & French, A. (2011). Covalent attachment of lysozyme to cotton/cellulose materials: Protein verses solid support activation. *Cellulose, 18*(5), 1239–1249. https://doi.org/10.1007/s10570-011-9563-6.

Fall, A. B., Lindström, S. B., Sundman, O., Ödberg, L., & Wågberg, L. (2011). Colloidal stability of aqueous nanofibrillated cellulose dispersions. *Langmuir, 27*(18), 11332–11338. https://doi.org/10.1021/la201947x.

Gull, N., Ishtikhar, M., Alam, M. S., Sabah Andrabi, S. N., & Khan, R. H. (2017). Spectroscopic studies on the comparative refolding of guanidinium hydrochloride denatured hen egg-white lysozyme and Rhizopus niveus lipase assisted by cationic single-chain/gemini surfactants via artificial chaperone protocol. *RSC Advances, 7*(45), 28452–28460. https://doi.org/10.1039/c6ra21528a.

Gustafsson, S., Manukyan, L., & Mihranyan, A. (2017). Protein – nanocellulose interactions in paper filters for advanced separation applications. *Langmuir, 33*, 4729–4736. https://doi.org/10.1021/acs.langmuir.7b00566.

Håkansson, K. M. O., Fall, A. B., Lundell, F., Yu, S., Krywka, C., Roth, S. V., … Söderberg, L. D. (2014). Hydrodynamic alignment and assembly of nanofibrils resulting in strong cellulose filaments. *Nature Communications, 5*, 4018–4027. https://doi.org/10.1038/ncomms5018.

Horn, D. W., Tracy, K., Easley, C. J., & Davis, V. A. (2012). Lysozyme dispersed single-walled carbon nanotubes: Interaction and activity. *The Journal of Physical Chemistry C, 116*(18), 10341–10348. https://doi.org/10.1021/jp300242a.

Huang, W., Wang, L., Wei, Y., Cao, M., Xie, H., & Wu, D. (2020). Fabrication of lysozyme/κ-carrageenan complex nanoparticles as a novel carrier to enhance the stability and in vitro release of curcumin. *International Journal of Biological Macromolecules, 146*, 444–452. https://doi.org/10.1016/j.ijbiomac.2020.01.004.

Josset, S., Orsolini, P., Siqueira, G., Tejado, A., Tingaut, P., & Zimmermann, T. (2014). Energy consumption of the nanofibrillation of bleached pulp, wheat straw and recycled newspaper through a grinding process. *Nordic Pulp and Paper Research Journal, 29*(1), 167–175. https://doi.org/10.3183/npprj-2014-29-01-p167-175.

Kim, Y. C., Late, S., Banga, A. K., Ludovice, P. J., & Prausnitz, M. R. (2008). Biochemical enhancement of transdermal delivery with magainin peptide: Modification of electrostatic interactions by changing pH. *International Journal of Pharmaceutics, 362*(1–2), 20–28. https://doi.org/10.1016/j.ijpharm.2008.05.042.

Klemm, D., Cranston, E. D., Fischer, D., Gama, M., Kedzior, S. A., Kralisch, D., … Rauchfuß, F. (2018). Nanocellulose as a natural source for groundbreaking applications in materials science: Today's state. *Materials Today, 21*(7), 720–748. https://doi.org/10.1016/j.mattod.2018.02.001.

Li, J., Zhang, Y., Fan, Q., Teng, C., Xie, W., Shi, Y., … Yang, Y. (2018). Combination effects of NaOH and NaCl on the rheology and gel characteristics of hen egg white proteins. *Food Chemistry, 250*(October 2017), 1–6. https://doi.org/10.1016/j.foodchem.2018.01.031.

Li, Z., Wang, Y., Pei, Y., Xiong, W., Xu, W., Li, B., … Li, J. (2017). Effect of substitution degree on carboxymethylcellulose interaction with lysozyme. *Food Hydrocolloids, 62*, 222–229. https://doi.org/10.1016/j.foodhyd.2016.07.020.

Li, Z., Xu, W., Zhang, C., Chen, Y., & Li, B. (2015). Self-assembled lysozyme/carboxymethylcellulose nanogels for delivery of methotrexate. *International Journal of Biological Macromolecules, 75*, 166–172. https://doi.org/10.1016/j.ijbiomac.2015.01.033.

Liu, X., Nielsen, L. H., Qu, H., Christensen, L. P., Rantanen, J., & Yang, M. (2019). Stability of lysozyme incorporated into electrospun fibrous mats for wound healing. *European Journal of Pharmaceutics and Biopharmaceutics, 136*(June 2018), 240–249. https://doi.org/10.1016/j.ejpb.2019.01.003.

Löbmann, K., & Svagan, A. J. (2017). Cellulose nanofibers as excipient for the delivery of poorly soluble drugs. *International Journal of Pharmaceutics, 533*(1), 285–297. https://doi.org/10.1016/j.ijpharm.2017.09.064.

Mallamace, D., Fazio, E., Mallamace, F., & Corsaro, C. (2018). The role of hydrogen bonding in the folding/unfolding process of hydrated lysozyme: A review of recent NMR and FTIR results. *International Journal of Molecular Sciences, 19*(12). https://doi.org/10.3390/ijms19123825.

Masruchin, N., Park, B. D., & Causin, V. (2018). Dual-responsive composite hydrogels based on TEMPO-oxidized cellulose nanofibril and poly(N-isopropylacrylamide) for model drug release. *Cellulose, 25*(1), 485–502. https://doi.org/10.1007/s10570-017-1585-2.

Mendoza, L., Batchelor, W., Tabor, R. F., & Garnier, G. (2018). Gelation mechanism of cellulose nanofibre gels: A colloids and interfacial perspective. *Journal of Colloid and Interface Science, 509*, 39–46. https://doi.org/10.1016/j.jcis.2017.08.101.

Meng, H., Xiao, P., Gu, J., Wen, X., Xu, J., Zhao, C., … Chen, T. (2014). Self-healable macro-/microscopic shape memory hydrogels based on supramolecular interactions. *Chemical Communications, 50*(82), 12277–12280. https://doi.org/10.1039/c4cc04760e.

Pei, Y., Li, Z., McClements, D. J., & Li, B. (2019). Comparison of structural and physicochemical properties of lysozyme/carboxymethylcellulose complexes and microgels. *Food Research International, 122*(December 2018), 273–282. https://doi.org/10.1016/j.foodres.2019.03.071.

Rol, F., Belgacem, M. N., Gandini, A., & Bras, J. (2019). Recent advances in surface-modified cellulose nanofibrils. *Progress in Polymer Science, 88*, 241–264. https://doi.org/10.1016/j.progpolymsci.2018.09.002.

Saito, T., Kimura, S., Nishiyama, Y., & Isogai, A. (2007). Cellulose nanofibers prepared by TEMPO-mediated oxidation of native cellulose. *Biomacromolecules, 8*(8), 2485–2491. https://doi.org/10.1021/bm0703970.

Shin, S., Park, S., Park, M., Jeong, E., Na, K., Youn, H. J., … Hyun, J. (2017). Cellulose nanofibers for the enhancement of printability of low viscosity gelatin derivatives. *BioResources, 12*(2), 2941–2954. https://doi.org/10.15376/biores.12.2.2941-2954.

Sudhakar, S., Santhosh, P. B., & Mani, E. (2017). Dual role of gold nanorods: Inhibition and dissolution of aβ fibrils induced by near IR laser. *ACS Chemical Neuroscience, 8*(10), 2325–2334. https://doi.org/10.1021/acschemneuro.7b00238.

Syngai, G. G., & Ahmed, G. (2019). Lysozyme: A natural antimicrobial enzyme of interest in food applications. *Enzymes in food biotechnology*. https://doi.org/10.1016/b978-0-12-813280-7.00011-6.

Tavakolian, M., Okshevsky, M., Van De Ven, T. G. M., & Tufenkji, N. (2018). Developing antibacterial nanocrystalline cellulose using natural antibacterial agents [Research-article]. *ACS Applied Materials & Interfaces, 10*(40), 33827–33838. https://doi.org/10.1021/acsami.8b08770.

Voutilainen, S., Paananen, A., Lille, M., & Linder, M. B. (2019). Modular protein architectures for pH-dependent interactions and switchable assembly of nanocellulose. *International Journal of Biological Macromolecules, 137*, 270–276. https://doi.org/10.1016/j.ijbiomac.2019.06.227.

Weishaupt, R., Siqueira, G., Schubert, M., Tingaut, P., Maniura-Weber, K., Zimmermann, T., … Ihssen, J. (2015). TEMPO-oxidized nanofibrillated cellulose as a high density carrier for bioactive molecules. *Biomacromolecules, 16*(11), 3640–3650. https://doi.org/10.1021/acs.biomac.5b01100.

Wu, T., Jiang, Q., Wu, D., Hu, Y., Chen, S., Ding, T., … Chen, J. (2019). What is new in lysozyme research and its application in food industry? A review. *Food Chemistry, 274*(September 2018), 698–709. https://doi.org/10.1016/j.foodchem.2018.09.017.

Wu, T., Zeng, Z., Siqueira, G., & De France, K. J. (2020). Dual-porous cellulose nanofibril aerogels via modular drying and cross-linking. *Nanoscale*. https://doi.org/10.1039/d0nr00860e. DOI: 10.1039/d0nr00860e.

Xu, C., Zhang Molino, B., Wang, X., Cheng, F., Xu, W., Molino, P., … Wallace, G. (2018). 3D printing of nanocellulose hydrogel scaffolds with tunable mechanical strength towards wound healing application. *Journal of Materials Chemistry B, 6*(43), 7066–7075. https://doi.org/10.1039/c8tb01757c.

Zhang, B., Sun, B., Li, X., Yu, Y., Tian, Y., Xu, X., … Jin, Z. (2015). Synthesis of pH- and ionic strength-responsive microgels and their interactions with lysozyme. *International Journal of Biological Macromolecules, 79*, 392–397. https://doi.org/10.1016/j.ijbiomac.2015.05.011.

Zhang, T., Zhou, P., Zhan, Y., Shi, X., Lin, J., Du, Y., … Deng, H. (2015). Pectin/lysozyme bilayers layer-by-layer deposited cellulose nanofibrous mats for antibacterial application. *Carbohydrate Polymers, 117*, 687–693. https://doi.org/10.1016/j.carbpol.2014.10.064.

Zhu, K., Ye, T., Liu, J., Peng, Z., Xu, S., Lei, J., … Li, B. (2013). Nanogels fabricated by lysozyme and sodium carboxymethyl cellulose for 5-fluorouracil controlled release. *International Journal of Pharmaceutics, 441*(1–2), 721–727. https://doi.org/10.1016/j.ijpharm.2012.10.022.

Zhu, Q., Yao, Q., Sun, J., Chen, H., Xu, W., Liu, J., … Wang, Q. (2020). Stimuli induced cellulose nanomaterials alignment and its emerging applications: A review. *Carbohydrate Polymers, 230*(July 2019), Article 115609. https://doi.org/10.1016/j.carbpol.2019.115609.